ELSEVIER

Polymer 44 (2003) 2177–2186

polymer

www.elsevier.com/locate/polymer

DFT study of hydrogenolysis as a chain transfer mechanism in olefin polymerisation catalysed by nickel-diimine-type catalysts

J. Ramos[a], A. Muñoz-Escalona[a], V. Cruz[b], J. Martínez-Salazar[a,*]

[a]*GIDEM, Instituto de Estructura de la Materia, CSIC Serrano 119, 28006 Madrid, Spain*
[b]*CTI, CSIC Pinar 19, 28006 Madrid, Spain*

Received 3 January 2003; received in revised form 22 January 2003; accepted 22 January 2003

Abstract

This report describes a computational DFT study, based on the hybrid density functional B3LYP method, designed to investigate the hydrogenolysis process that occurs in ethylene polymerisation catalysed by a nickel-bulk diimine catalyst (*N*,*N*′-bis(2,6-diisopropylphenyl)-2,3-butanediimine nickel(II) methyl cation [{(2,6-(^{i}Pr)$_2$Ph)N=C(Me)–C(Me) = N(2,6-(^{i}Pr)$_2$Ph)}NiCH$_3$]$^+$. Mechanisms of ethylene and hydrogen insertions into the growing polymer chain and ethylene insertion into the hydride complex formed after hydrogenolysis were investigated. The results obtained for these catalysts were then compared to those calculated for metallocene catalysts. Due to a higher difference in energy barriers between ethylene and hydrogen insertion, it may be concluded that controlling the molecular weight of the resultant polymer using nickel diimine catalysts is even more difficult than for the metallocene catalysts. Through statistical thermodynamics and kinetics calculations it was shown that the activity and molecular weights of polymers produced by nickel-diimine catalysts are dramatically decreased in the presence of hydrogen with respect to those of polymers generated by metallocene catalysts. These findings help to clarify the contradictory experimental results published in the scientific and technical literature regarding the effect of hydrogen on the catalytic activity and molecular weight of polymers produced using nickel diimine catalysts.

Keywords: Hydrogenolysis; Nickel diimine catalysts; Density functional study

1. Introduction

Single-site homogeneous catalysts have been receiving considerable attention over traditional Ziegler–Natta multi-site heterogeneous catalysts due to their superior performance in olefins polymerisation. Particularly, metallocene catalysts are widely used in olefin polymerisation [1–6] and the polymerisation reactions with these catalysts have been extensively described both from an experimental and theoretical perspective [1–3,7–14]. Recently, diimine nickel (II) complexes are emerging as an alternative group of homogeneous catalysts for olefin polymerisation. Most of the works published on metallocene catalyst deal with the influence of the different types of catalysts structure on the polymerisation mechanism, catalytic activity and microstructure of the resulting polymers. However, much less attention has been paid to the effect of hydrogen in controlling polymer molecular weight, given the importance of the hydrogenolysis process in the polyolefin industry.

It is well known that the hydrogenolysis reaction is a chain transfer mechanism that regulates polymer molecular weight in olefin polymerisation. However, the use of the nickel-diimine catalyst for this reaction has been related to highly contradictory results in the technical and scientific literature. Dupont's researchers evaluated ethylene polymerisation in the presence of molecular hydrogen using the (*N*,*N*′-bis(2,6-diisopropylphenyl)-2,3-butanediimine nickel(II) dibromide (**1**) catalyst activated with MAO. These authors noted that the activity of the catalyst was unaffected when molecular hydrogen was present in the polymerisation reactor. They also found a drastic decrease in polyethylene molecular weight from about 2×10^6 to 7×10^4 g/mol in the presence of around 20% hydrogen [15]. Neto et al. [16] also described that hydrogen could control the molecular weight of polyethylenes obtained using the 1,4-bis(2,6-diisopropyl-phenyl)acenaphetediimine–nickel(II) dichloride (**2**) catalyst activated with triisobutylaluminium

* Corresponding author. Tel.: +34-915901618; fax: +34-915855413.
E-mail address: jmsalazar@iem.cfmac.csic.es (J. Martínez-Salazar).

0032-3861/03/$ - see front matter © 2003 Elsevier Science Ltd. All rights reserved.
doi:10.1016/S0032-3861(03)00057-0

(TIBA). These authors, nevertheless, reported a marked drop in the productivity of the catalyst, besides the diminished molecular weight of the resultant polymers, when hydrogen was present in the gas feed. Similar results were published by Muñoz-Escalona et al. [17] using nickel-diimine catalysts activated with MAO as a cocatalyst.

Several studies have focused on ethylene insertion and chain transfer mechanisms in nickel-diimine catalyst systems [18–23]. These works have been based either on the use of the IMOMM scheme or simplified catalyst models to explore these complex systems. In the present study we report results obtained using the all-electron hybrid DFT method. To the best of our knowledge, there are only two published papers that theoretically deal with the hydrogenolysis process using metallocene catalysts [14,24]. Yet to date, the theoretical role of hydrogen in controlling the molecular weight of polyethylenes produced using nickel-diimine catalysts has not been explored. The results reported here may shed light on the controversial findings described above.

2. Computational methods

Geometries, energies and vibrational frequencies for the reactants, transition states and products of the different reactions were calculated using the B3LYP DFT hybrid model [26] implemented in the GAUSSIAN98 computer package [25]. This model has been shown to be fairly reliable for geometry and energy calculations [27].

Besides DFT correlation terms, the method includes a mixture of Hartree–Fock and DFT exchange data and takes the form:

$$E^{\mathrm{XC}}_{\mathrm{B3LYP}} = AE^{\mathrm{Slater}}_{\mathrm{X}} + (1-A)E^{\mathrm{HF}}_{\mathrm{X}} + B\Delta E^{\mathrm{B88}}_{\mathrm{X}} + E^{\mathrm{VWN}}_{\mathrm{C}} + C\Delta E^{\mathrm{LYP}}_{\mathrm{C}} \quad (1)$$

The local correlation terms are given by the Vosko, Wilk, Nusair 1980 ($E^{\mathrm{VWN}}_{\mathrm{C}}$) [28] and Lee, Yang and Parr ($\Delta E^{\mathrm{LYP}}_{\mathrm{C}}$) [29] functionals, the latter including non-local correction terms. The exchange terms are given by a combination of Slater ($E^{\mathrm{Slater}}_{\mathrm{X}}$) [30] and Becke ($\Delta E^{\mathrm{B88}}_{\mathrm{X}}$) [31] as well as Hartree–Fock (E^{HF}_{X}) exchange functionals. Constants A, B and C were determined according to Becke by fitting to the G1 molecule set.

The Los Alamos ECP plus DZ (LANL2DZ) [32–34] basis set was used for all atoms. This basis set makes use of effective core potentials for the innermost electrons and takes into account relativistic effects in post-third-row atoms.

Transition state geometries were determined by the Synchronous Transit-Guided Quasy-Newton (STQN) [35] method to locate a saddle-point in the reactant-to-product path. The nature of the stationary points found was checked by frequency calculations.

Thermodynamics data calculations were performed at 298.15 K and 1 atm of pressure using standard statistical thermodynamic methods implemented in the GAUSSIAN98 package [36]. Imaginary frequencies for the transition states were neglected in all the calculations. No symmetry or constraints were used.

Evaluation of a relative population was based on Boltzmann statistics using the standard equation:

$$\frac{n_i}{N} = \frac{\exp(-G_i/kT)}{\sum_j \exp(-G_j/kT)} \quad (2)$$

where n_i is the population at energy level i, N is the total population, G_i is the Gibb's free energy corresponding to level i, k is the Boltzmann constant and T the absolute temperature. The n_i/N ratio is related to the probability of finding a molecule at energy level i. Equilibrium conditions were assumed when applying the statistical thermodynamics, although the experimental work was not considered a priori in the equilibrium state.

To reduce the computational effort, the growing polymer chain was represented by a methyl group.

3. Results and discussion

Scheme 1 shows the ethylene and hydrogen insertion mechanisms considered in this study. According to the Brookhart–Green mechanism [37], ethylene coordinates to cationic active specie **I** to form a π-complex **II**, which undergoes insertion through transition state **III** yielding a γ-agostic insertion product **IV**. This structure can develop to form a more stable β-agostic conformer **V**. In the molecular hydrogen insertion process, the dihydrogen complex **VI** is formed in the first step and the reaction occurs through transition state **VII** to give the corresponding hydrogenolysis product **VIII**. This adduct can subsequently form a hydride cation **IX** and a saturated alkyl chain, which is ejected from the active site. A new ethylene monomer can be inserted into structure **IX** and a new polymer chain starts to grow.

In this study, the energy profiles for all calculated reactions are discussed in terms of Gibb's free energy rather than electronic energy. This enables temperature and entropic effects to be taken into account.

3.1. Ethylene insertion

Structures for the different stationary points (**I**–**V**) along the ethylene insertion pathway are shown in Fig. 1. Selected geometrical parameters are given in Table 1. Fig. 2 shows the corresponding Gibb's free energy profile.

The first step in the ethylene insertion process is the formation of a π-complex. In the most stable π-complex found, the ethylene monomer is oriented in a direction perpendicular to the Ni–C3 bond (Ni–C3–C2–C1 angle 77.1°, Table 1) and is coordinated symmetrically to the

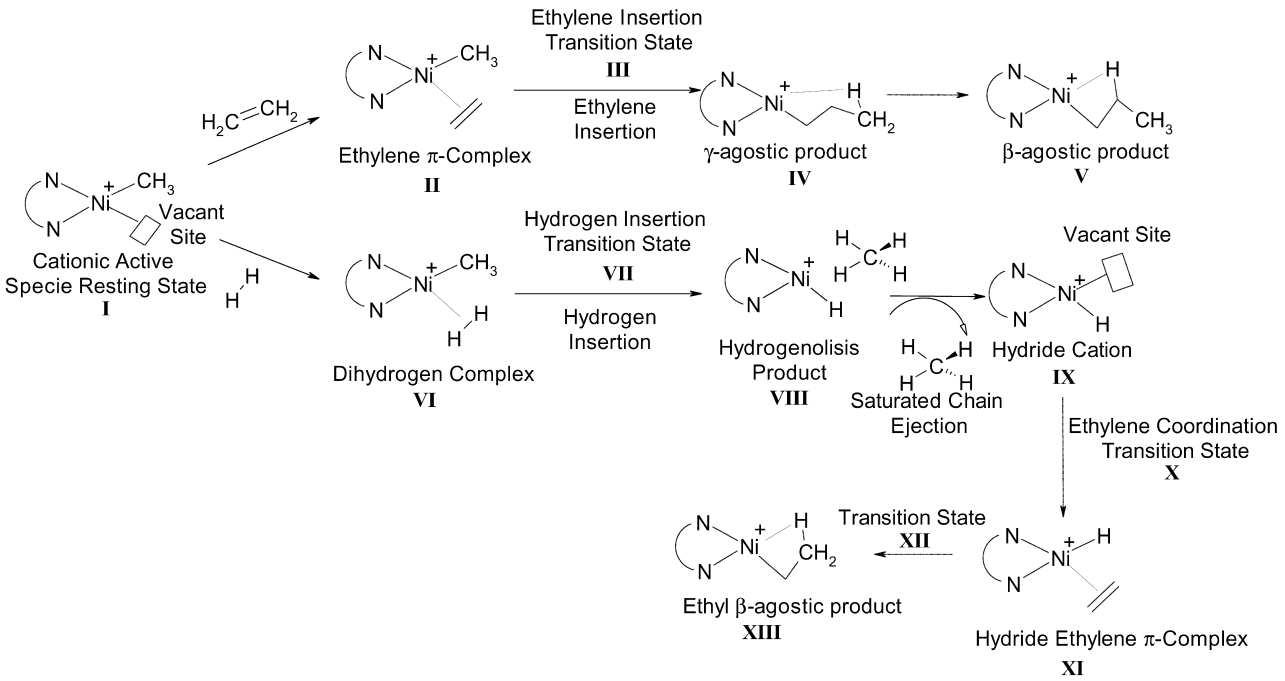

Scheme 1.

metal atom (Ni–C1 and Ni–C2 distances 2.154 and 2.156 Å, Table 1). The distance Ni–C3 is 0.048 Å larger than in the methyl cationic active site **I** indicating a weaker Ni–C3 bond in complex **II**. A structure showing a parallel orientation of ethylene with respect to the metal alkyl bond was also found. This parallel π-complex was less stable than the perpendicular structure **II** by 10.7 kcal/mol and was not considered further. The free energy of ethylene coordination to the methyl cationic active species **I** was −3.1 kcal/mol. The reaction proceeds through transition state **III**, which is 12.7 kcal/mol above **II**. Experimental Gibb's free energy barriers for ethylene insertion in these nickel complexes are

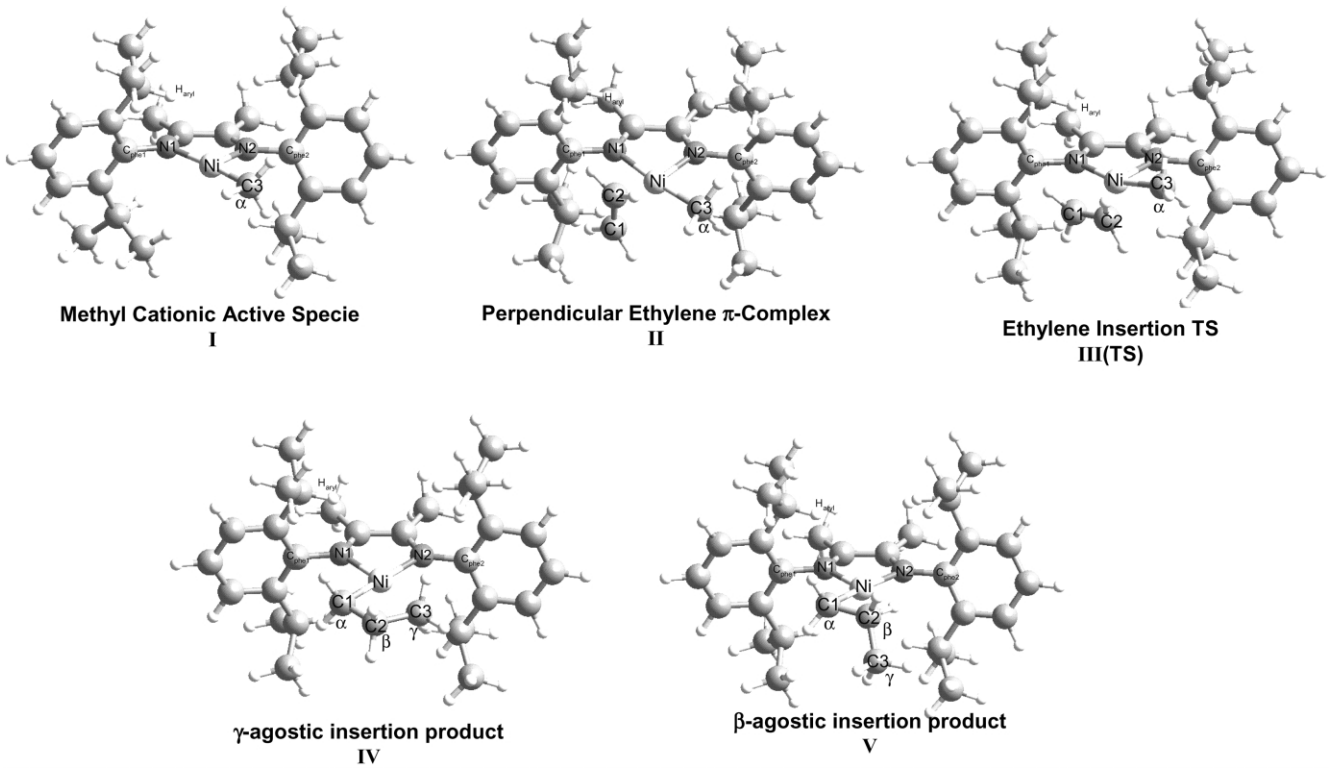

Fig. 1. Optimised structures for the ethylene insertion reaction into the methyl cationic active species (**I**).

Table 1
Selected geometrical parameters for calculated structures of the ethylene insertion reaction into the methyl cationic active specie (I). Distances are given in angstroms and angles in degrees

Parameter	Methyl cationic active specie **I** + ethylene	Perpendicular ethylene π-complex **II**	Ethylene insertion TS **III**(TS)	γ-Agostic insertion product **IV**	β-Agostic insertion product **V**
Ni–C3	1.883	1.931	2.064	2.299	3.367
Ni–N1	1.963	2.055	1.967	1.903	1.909
Ni–N2	1.893	1.987	2.023	2.010	1.968
Ni–Hα[a]	2.324 (1.112)	2.463 (1.096)	2.276 (1.099)	**2.089** (**1.113**)[b]	**1.738** (**1.185**)[c]
Ni–H(aryl)[d]	2.680 (1.102)	3.233 (1.099)	2.965 (1.099)	3.083 (1.099)	2.914 (1.099)
Ni–$C_{phe}1$[e]	1.447	1.462	1.464	1.461	1.459
Ni–$C_{phe}2$[e]	1.458	1.465	1.461	1.452	1.453
Ni–C1	–	2.154	1.975	1.931	1.903
Ni–C2	–	2.156	2.295	2.603	2.227
C1–C2	1.348	1.383	1.416	1.535	1.503
C2–C3	–	2.878	2.145	1.561	1.542
N2–N1–C3	101.9	92.2	91.9	98.5[f]	104.0[f]
$\varphi 1$[g]	73.6	88.8	77.7	106.7	103.2
$\varphi 2$[g]	86.5	90.9	78.9	78.6	76.9
Ni–C3–C2–C1	–	77.1	−4.6	−1.3	68.0
N2–C–C–N1[f]	2.1	−1.1	−7.1	3.0	3.6

Labelling of atoms as indicated in Fig. 1.

[a] Shortest Ni–Hα distance. Corresponding C–H distances are given in parentheses. Numbers in bold indicate agostic interactions.

[b] In species **IV**, Hα atoms occupy the γ position.

[c] In specie **V**, Hα atoms occupy the γ position.

[d] Shortest Ni–H(aryl) distance. Corresponding C–H distances are given in parentheses. Numbers in bold indicate agostic interactions.

[e] Carbon atoms attached to the N1 and N2 atoms, respectively.

[f] N1–Ni–C1 angle. This dihedral angle reflects 'puckering' of the diimine ligand.

[g] These angles indicate aryl group positions with respect to the diimine plane. Values close to 90° indicate the aryl groups are perpendicular to the diimine plane.

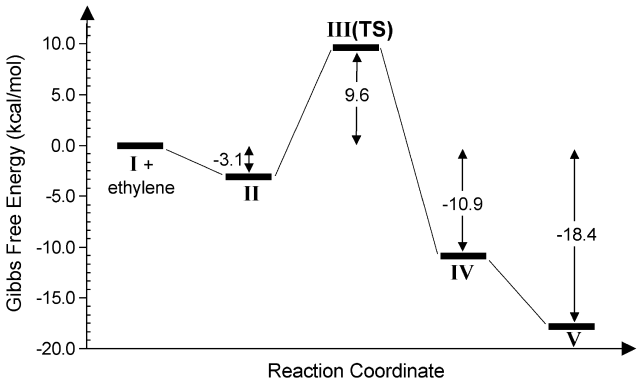

Fig. 2. Gibb's free energy profile for the ethylene insertion reaction into the methyl cationic active specie (**I**). Species labels are provided in Fig. 1 and Scheme 1. All energies are expressed in relation to **I** + ethylene.

in the range 13–14 kcal/mol [38], in good agreement with the theoretical Gibb's free energy barrier obtained.

Transition state **III** evolves to the γ-agostic insertion product **IV**. This product is −7.8 kcal/mol more stable than the perpendicular π-complex **II**. Complex **IV** is characterised by an agostic interaction between a Hγ atom in the alkyl chain and the nickel atom (2.089 and 1.113 Å for Ni–Hγ and C–Hγ distances, respectively, Table 1). Further, the alkyl chain is almost coplanar with the equatorial plane of the catalyst (Ni–C3–C2–C1 angle −1.3°, Table 1).

The most stable conformer found for the ethylene insertion product is, however, the β-agostic structure **V**, which is 7.5 kcal/mol below the γ-agostic conformer. Complex **V** shows intense β-agostic interaction (Ni–Hβ and C–Hβ distances of 1.738 and 1.185 Å, respectively, Table 1).

3.2. Hydrogen insertion

The optimised structures found for the molecular hydrogen insertion process are shown in Fig. 3, along with the geometrical parameters in Table 2. The corresponding free energy profile is given in Fig. 4.

When entropic effects are considered, the most stable dihydrogen complex **VI** calculated is 4.1 kcal/mol higher in free energy than the independent reactants. The situation is reversed when the electronic effect alone is considered, as usually done in theoretical calculations [20–22,24]. The hydrogen molecule aligns in a parallel manner to the metal alkyl bond (Ni–C3–H2–H1 torsion angle −2.3°, see Table 2) and contrasts with the perpendicular ethylene coordination observed in the π-complex **II**. This could be due to a demand for more steric room for the ethylene monomer compared to the hydrogen molecule.

The transition state **VII** obtained for the insertion process was 6.1 kcal/mol above the free energy calculated for the separate species and only 2.0 kcal/mol above that of complex **VI**. These results suggest the hydrogen insertion reaction occurs without the formation of a dihydrogen complex.

The hydrogenolysis insertion product **VIII** is composed of a hydride cation and a methane molecule, which are bound by two agostic interactions (Ni–Hα 1.978 and Ni–H2 1.946 Å, see Table 2). The reaction energy is −6.9 kcal/mol with respect to the separate species considered as the reactant. The saturated chain can be ejected from the coordination sphere to give rise to the hydride cation **IX** and one methane molecule. The chain ejection process (simplified as a methane molecule) is exothermic by 4.3 kcal/mol with respect to **VIII**. One of the ancillary aryl rings in the hydride cation IX rotates around the N2–C_{phe2} bond (see φ2 angle in Table 2) to form an agostic interaction between the H_{aryl} and Ni atoms (1.702 and 1.145 Å for the Ni–H_{aryl} and C_{aryl}–H_{aryl} distances, respectively, see Table 2). In principle, the active site could be partially blocked by this agostic interaction. This possibility was explored by performing calculations on the ethylene coordination and insertion processes in hydride cation **IX**. These results are reported in Section 3.3.

3.3. Ethylene insertion in the hydride cation

The whole insertion reaction was divided into two steps: ethylene coordination and insertion. The structures found for the different stationary points of the complete process are shown in Fig. 5, while some of the geometrical parameters are given in Table 3. Fig. 6 shows the corresponding free energy profile.

An incoming ethylene monomer can be easily coordinated to the hydride cation **IX**, as may be observed in Fig. 6. Complex formation occurs through the transition state **X**, which is only 0.5 kcal/mol above that of the individual reactants. The geometry of the transition state reveals that the aryl ring rotates to adopt a more perpendicular position with respect to the **IX** specie (φ2 from 26.3° to 53.9°, see Tables 2 and 3). Agostic interaction between the ancillary ligand and the metal atom is weakened by the aryl rotation (Ni–H_{aryl} from 1.702 to 2.152 Å).

The hydride π-complex **XI** formed in the coordination step was 11.4 kcal/mol more stable than the individual reactants (see Fig. 6). In the corresponding structure, the ethylene monomer lies perpendicular to the Ni–H bond (Ni–H1–C2–C1 angle −82.0°) in a similar fashion to the methyl ethylene π-complex **II**.

The ethylene monomer can be further inserted into the Ni–H1 bond through transition state **XII**, which is only 0.4 kcal/mol above the hydride π-complex **XI**. The geometry of the saddle point closely resembles that of the reactant, except for the relative orientation of the ethylene monomer with respect to the Ni–H1 bond (Ni–H1–C2–C1 angle from −82.0° to −52.3°).

The final product **XIII** obtained after the insertion process has taken place shows a β-agostic interaction (Ni–H1 1.770 Å, see Table 3). This structure is −17.9 kcal/mol more stable than the **XI** complex.

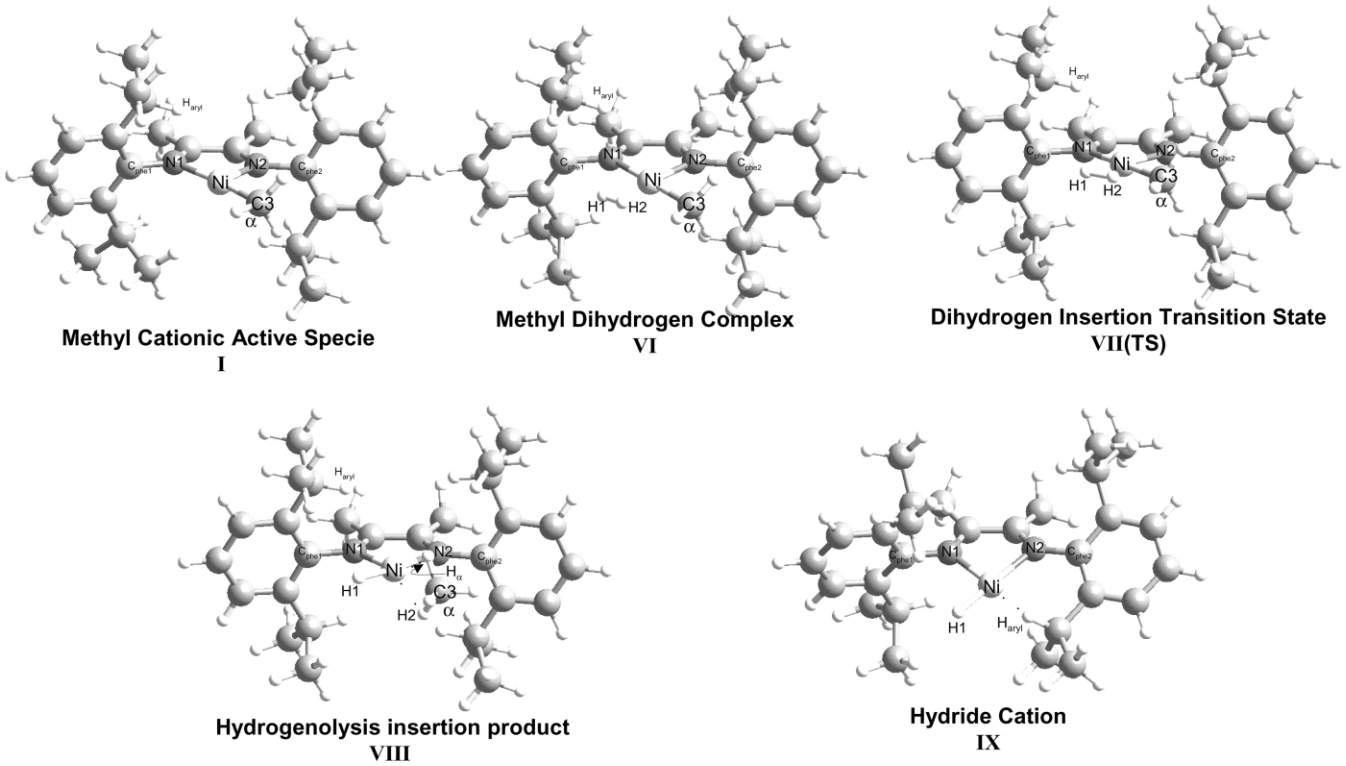

Fig. 3. Optimised structures for the hydrogen insertion reaction into the methyl cationic active species (**I**).

3.4. Comparison with metallocene-catalysed hydrogenolysis

As mentioned in the foregoing sections, the hydrogen and ethylene monomers compete for cationic active specie **I**. The activation energy obtained for hydrogen insertion into **I** was 6.6 kcal/mol lower than that corresponding to the ethylene insertion (see Figs. 2 and 4). A difference of only 3.8 kcal/mol was obtained for similar reactions in the metallocene $Cp_2ZrCH_3^+$ catalytic system [14]. These results indicate that hydrogen insertion is more favourable than ethylene insertion in the nickel cationic species **I** with respect to the metallocene cationic specie. However, it should be taken into account that a binding complex needs to form before the insertion process can take place. The formation of this complex is much more favourable in the case of ethylene than hydrogen (see Figs. 2 and 4) such that ethylene oligomerisation/polymerisation should be observed depending on the relative values of the coordination and insertion energies. Applying Boltzmann statistics and the transition-state theory yields useful information in that the effect of adding hydrogen on polymerisation activity can be quantified. This was undertaken in a previous study for metallocene catalysts [14].

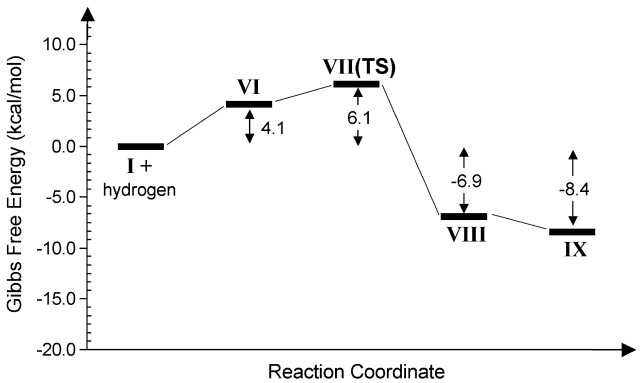

Fig. 4. Energy profile for the hydrogen insertion reaction into the methyl cationic active specie (**I**). Species labels are provided in Fig. 3 and Scheme 1. All energies are expressed in relation to **I** + hydrogen.

The population ratio between ethylene π-complex **II** and dihydrogen complex **VI** can be calculated using the following equation:

$$\frac{n_{\mathbf{II}}}{n_{\mathbf{VI}}} = \frac{\exp(-\Delta G_{\mathbf{I}+\text{Ethylene}\rightarrow\mathbf{II}}/RT)}{\exp(-\Delta G_{\mathbf{I}+\text{Hydrogen}\rightarrow\mathbf{II}}/RT)} \tag{3}$$

where $n_{\mathbf{II}}$ and $n_{\mathbf{VI}}$ are the populations in the ethylene and hydrogen complexes, respectively. Further, based on this population ratio and the free energy barriers ($\Delta G^{\#}$), the probability ratio of ethylene to hydrogen insertion can be calculated according to the following equation:

$$\frac{P_{C_2H_4}}{P_{H_2}} = \frac{\frac{n_{\mathbf{II}}}{n_{\mathbf{VI}}}\exp(-\Delta G^{\#}_{\mathbf{II}\rightarrow\mathbf{IV}}/RT)}{\exp(-\Delta G^{\#}_{\mathbf{VI}\rightarrow\mathbf{VIII}}/RT)} \tag{4}$$

where $P_{C_2H_4}/P_{H_2}$ is the probability ratio of ethylene per hydrogen insertion. Based on the experiments published by Blom et al. [4], describing batch ethylene polymerisation in the presence of hydrogen and using metallocene catalysts,

Table 2
Selected geometrical parameters for calculated structures in the hydrogen insertion reaction into methyl cationic active specie (I). Distances are given in angstroms and angles in degrees

Parameter	Methyl cationic active specie (**I**) + hydrogen	Methyl dihydrogen complex (**VI**)	Hydrogen insertion TS (**VII**)	Hydrogenolysis insertion product (**VIII**)	Hydride cation (**IX**) + methane
Ni–Cα	1.883	1.948	2.036	2.296	n.a
Ni–N1	1.963	1.978	1.932	1.884	1.880
Ni–N2	1.893	1.934	1.958	1.996	1.950
Ni–Hα[a]	2.324 (1.112)	2.460 (1.096)	2.439 (1.093)	**1.978** (**1.111**)	–
Ni–H(aryl)[b]	2.680 (1.102)	2.747 (1.102)	2.826 (1.100)	2.903 (1.100)	**1.702** (**1.145**)
Ni–$C_{phe}1$[c]	1.447	1.455	1.458	1.462	1.455
Ni–$C_{phe}2$[c]	1.458	1.461	1.459	1.455	1.430
Ni–H1	–	1.733	1.571	1.465	1.472
Ni–H2	–	1.706	1.571	**1.946**	–
H1–H2	0.746	0.783	0.955	2.319	–
H2–Cα	–	2.134	1.542	1.113	–
N2–N1–Cα	101.9	94.8	97.7	99.6	93.8[d]
$\varphi 1$[e]	73.6	75.0	77.8	82.4	78.7
$\varphi 2$[e]	86.5	88.5	86.1	80.1	26.3
Ni–Cα–H2–H1	–	−2.3	0.0	−39.0	–
N2–C–C–N1[f]	2.1	2.5	2.2	2.5	−7.0

Labelling of atoms as indicated in Fig. 3.

[a] Shortest Ni–Hα distance. Corresponding C–H distances are given in parentheses. Numbers in bold indicate agostic interactions.

[b] Shortest Ni–H(aryl) distance. Corresponding C–H distances are given in parentheses. Numbers in bold indicate agostic interactions.

[c] Carbon atoms attached to the N1 and N2 atom, respectively.

[d] N2–N1–Hα angle.

[e] These angles give an idea of aryl group positions with respect to the diimine plane. Values close to 90° indicate the aryl groups remain perpendicular to the diimine plane.

[f] This dihedral angle reflects puckering of the diimine ligand.

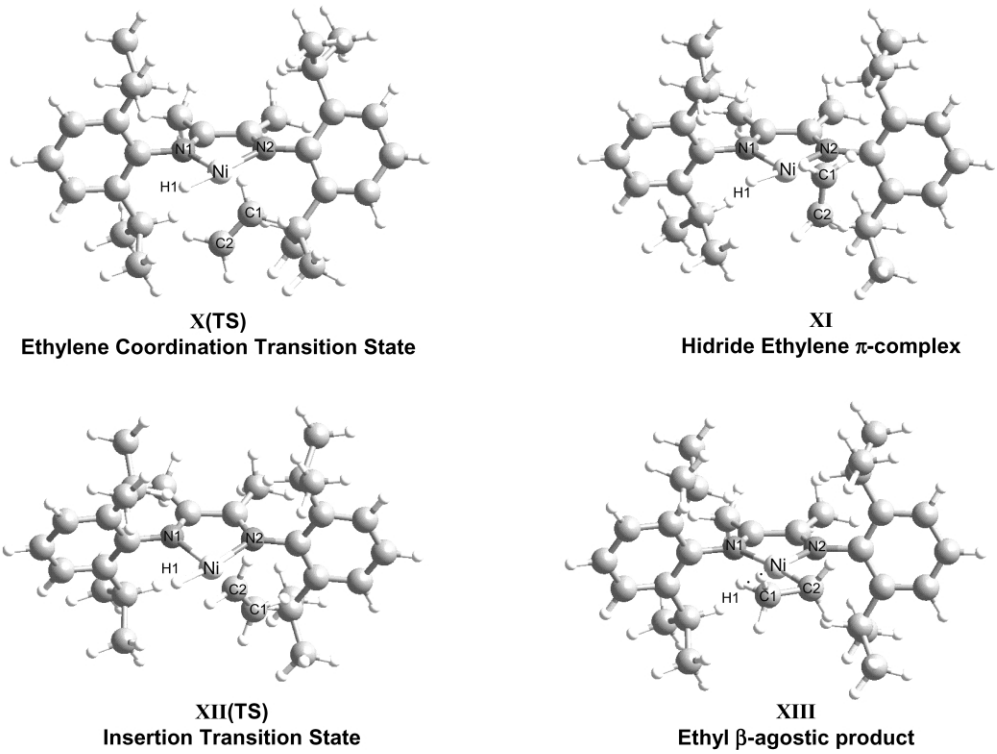

Fig. 5. Optimised structures for ethylene coordination and subsequent insertion to the hydride cation **IX**.

Fig. 7 shows a plot of predicted molecular weight against the percentage of hydrogen consumed during the reaction process for metallocene and nickel-diimine catalysts. These calculations are similar to those already published by us using metallocene catalysts [14]. For the calculation, it has been assumed the same number of ethylene and hydrogen molecules at the reaction start. As the reaction proceeds, the remaining hydrogen percentages are introduced in Eq. (4) by an appropriate constant which indicates the ethylene/hydrogen ratio during the polymerisation process. The predicted molecular weights undergo an exponential drop with the percentage of consumed hydrogen. This closely resembles the experimental results reported by Neto et al. [16].

Table 3
Selected geometrical parameters for calculated structures in ethylene coordination to hydrogen insertion products. Distances are given in angstroms and angles in degrees

Parameter	**X**-TS	**XI**	**XII**-TS	**XIII**
Ni–N1	1.873	1.930	1.922	1.968
Ni–N2	1.980	2.028	2.027	1.905
Ni–H(aryl)[a]	**2.153** (**1.115**)	3.052 (1.100)	2.900 (1.099)	2.723 (1.102)
Ni–$C_{phe}1$[b]	1.458	1.460	1.462	1.453
Ni–$C_{phe}2$[b]	1.440	1.458	1.458	1.459
Ni–H1	1.466	1.457	1.452	1.770
Ni–C1	3.661	2.149	2.192	1.898
Ni–C2	3.753	2.155	2.130	2.210
C2–H1	3.043	2.483	2.206	1.170
C1–C2	1.351	1.382	1.385	1.507
N1–Ni–H1	91.8	89.8	88.2	104.2[c]
$\varphi 1$	86.3	99.4	81.2	74.9
$\varphi 2$	53.9	84.2	85.3	83.8
Ni–H1–C2–C1	−134.3	−82.0	−52.3	0.3
N2–C–C–N1[d]	−1.1	2.9	3.1	3.2

Labelling of atoms as indicated in Figs. 5 and 6.
[a] Corresponding C–H distances are in parentheses. Numbers in bold indicate agostic interactions.
[b] Carbon atoms attached to the N1 and N2 atoms, respectively.
[c] N2–Ni–Cα angle.
[d] This dihedral angle reflects puckering of the diimine ligand.

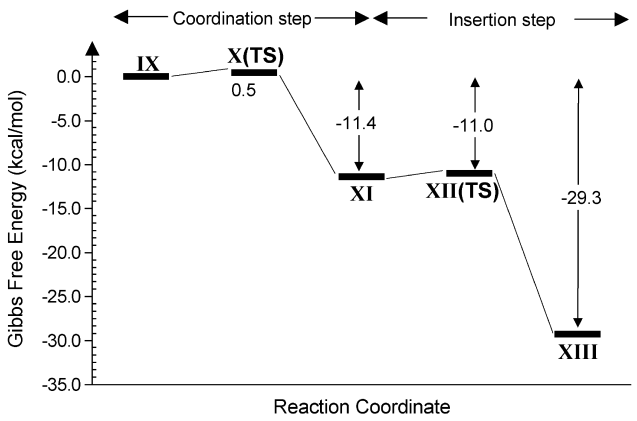

Fig. 6. Energy profile for ethylene coordination and insertion into the hydride cation. Species labels are provided in Fig. 5 and Scheme 1. All energies are expressed in relation to **IX** + ethylene.

Fig. 7 shows that the nickel-diimine catalyst system is more sensitive to the presence of molecular hydrogen than metallocene systems. This leads to the concept that, all other things equal, polymer molecular weights for the nickel-diimine catalyst are about two orders of magnitude lower than the products of the metallocene catalyst system.

The low molecular weights obtained during polymerisation in the presence of hydrogen indicate the formation of oligomers, which would probably not give rise to a polyethylene product, thus yielding very low activity measurements. These data could explain the lack of polymerisation activity related to the use of a nickel-diimine catalyst in experimental work when molecular hydrogen was added to the reaction vessel [17]. Depressed activity has also been reported experimentally by Neto et al. [16]. In the case of metallocene catalysts, a significant drop in activity would not be expected since relatively higher molecular weight polymers are formed in the presence of hydrogen. In contrast using the nickel-diimine system, lower molecular weight oligomers are formed and these cannot form a polyethylene product yielding low polymerisation activity.

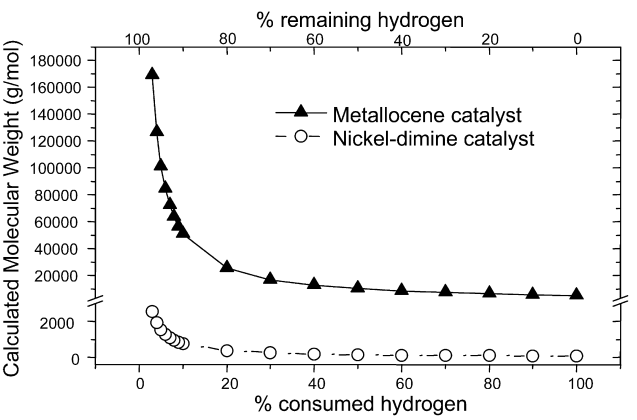

Fig. 7. Molecular weight calculated as a function of the percentage of hydrogen remaining (see text for details).

4. Conclusions

The following conclusions can be drawn from the present findings:

Hydrogenolysis is a highly effective chain transfer process in ethylene polymerisation using nickel-diimine catalysts. Insertion of a hydrogen molecule into the Ni–C bond is associated with a low Gibb's free energy barrier (6.1 kcal/mol). This energy barrier is even lower than that corresponding to ethylene insertion (12.7 kcal/mol). However, the polymerisation reaction is still possible since the ethylene forms a reactant π-complex (**II**) which is much more stable than the corresponding dihydrogen complex (**VI**). Thus, the population of **II** complexes is higher that of the **VI** complexes, leading to an increased probability of ethylene insertions compared to hydrogen insertions. The hydride complex formed after hydrogen insertion can easily trigger the formation of a new polymer chain, since there are no substantial barriers for the coordination and insertion of an incoming ethylene monomer.

Polymer molecular weight calculated according to the percentage of hydrogen consumed shows similar behaviour to results found experimentally [16,17]. The data reported here suggest a considerable drop in activity and molecular weight, in agreement with experimental results determined under polymerisation conditions.

The nickel-diimine system is much more sensitive to molecular hydrogen than the metallocene catalyst specie. Thus, controlling molecular weight by hydrogen addition in the nickel-diimine catalyst system is even more difficult than in the metallocene catalyst system.

Acknowledgements

Thanks are due to the MCYT (Grant MAT2002-01242) for funding this investigation. The authors also acknowledge Repsol-YPF, Spain for their permission to publish these data.

References

[1] Soares JBP, Hamielec AE. Polym React Engng 1995;3(2):131–200.
[2] Brintzinger HH, Fischer D, Mülhaupt R, Rieger B, Waymouth RM. Angew Chem Int Ed Engl 1995;34:1143.
[3] Kaminsky W, Sinn H. Transition metals and organometallics for catalysts for olefin polymerisation. New York: Springer; 1988.
[4] Blom R, Dahl IM. Macromol Chem Phys 1999;200:442.
[5] Kamisnky W, Lüker H. Makromol Chem, Rapid Commun 1984;5:225.
[6] D'Agnillo L, Soares JBP, Penlidis A. Macromol Chem Phys 1998;199:955.
[7] Kawamura-Kuribayashi H, Koga N, Morokuma K. J Am Chem Soc 1992;114(19):8687–94.
[8] Meier RJ, Van Doremaele GHJ, Iarlori S, Buda F. J Am Chem Soc 1994;116(16):7274–81.

[9] Yoshida T, Koga N, Morokuma K. Organometallics 1995;14(2):746–58.
[10] Cruz VL, Muñoz-Escalona A, Martínez-Salazar J. Polymer 1996;37(9):1663–7.
[11] Woo TK, Margl PM, Lohrenz JCW, Blöchl PE, Ziegler T. J Am Chem Soc 1996;118(51):13021–30.
[12] Cruz VL, Muñoz-Escalona A, Martínez-Salazar J. J Polym Sci, Part A: Polym Chem 1998;36(7):1157–67.
[13] Muñoz-Escalona A, Ramos J, Cruz VL, Martínez-Salazar J. J Polym Sci, Part A: Polym Chem 2000;38(3):571–82.
[14] Ramos J, Cruz VL, Muñoz-Escalona A, Martínez-Salazar J. Polymer 2000;41(16):6161–9.
[15] Arthur SD, McLain SJ. International Application PCT W0 99/61492; 2nd December 1999.
[16] Rochefort Neto OI, Mauler RS, Souza RF. Macromol Chem Phys 2001;202:3232–6.
[17] Muñoz-Escalona A, Méndez L, Sancho J, Lafuente P, Peña B, Michiels W, Hidalgo G, Martínez-Nuñez MF. International Symposium on Catalyst for Synthesis and Polymerisation, Hamburg, Germany; September 1998.
[18] Musaev DG, Froese RDJ, Svensson M, Morokuma K. J Am Chem Soc 1997;119(2):367–74.
[19] Strömberg S, Zetterberg K, Sieghbahn PEM. J Chem Soc Dalton Trans 1997;4147.
[20] Deng L, Margl P, Zeigler T. J Am Chem Soc 1997;119(5):1094–100.
[21] Deng L, Woo TK, Cavallo L, Margl PM, Zeigler T. J Am Chem Soc 1997;119(26):6177–86.
[22] Froese RDJ, Musaev DG, Morokuma K. J Am Chem Soc 1998;120(7):1581–7.
[23] Ramos J, Cruz V, Muñoz-Escalona A, Martínez-Salazar J. Polymer 2001;42:8019–23.
[24] Petitjean L, Pattou D, Ruiz-López MF. Tetrahedron 2001;57:2769–74.
[25] Frisch MJ, Trucks GW, Schlegel HB, Scuseria GE, Robb MA, Cheeseman JR, Zakrzewski VG, Montgomery JA, Stratmann RE, Burant JC, Dapprich S, Millan JM, Daniels AD, Kudin KN, Strain MC, Farkas O, Tomasi J, Barone V, Cossi M, Cammi R, Mennucci B, Pomelli C, Adamo C, Clifford S, Petersson GA, Ayala PY, Cui Q, Morokuma K, Malick DK, Rabuk AD, Raghavachari K, Foresman JB, Ciolowski J, Ortiz JV, Stefanov BB, Liu G, Liashenko A, Piskorz P, Komaromi I, Gomperts R, Martin RL, Fox DJ, Keith TA, Al-Laham MA, Peng CY, Nanayakkara A, Gonzalez C, Challacombe M, Gill PMW, Johnson BG, Chen W, Wong MW, Andres JL, Head-Gordon M, Reploge ES, Pople JA. GAUSSIAN98 (Revision A.1), Gaussian Inc., Pittsburgh, PA; 1998.
[26] Becke AD. J Chem Phys 1993;98:5648.
[27] Froese RDJ, Musaev DG, Matsubara T, Morokuma K. J Am Chem Soc 1997;119:7190.
[28] Vosko H, Wilk L, Nusair M. Can J Phys 1980;58:1200.
[29] Lee C, Yang W, Parr RG. Phys Rev B 1988;37:785.
[30] Slater JC. The self-consistent field for molecular and solids. Quantum theory of molecular and solids, vol. 4. New York: McGraw-Hill; 1974.
[31] Becke AD. Phys Rev A 1988;38:3098.
[32] Hay PJ, Wadt WR. J Chem Phys 1985;82:270.
[33] Wadt WR, Hay PJ. J Chem Phys 1985;82:284.
[34] Hay PJ, Wadt WR. J Chem Phys 1985;82:299.
[35] Peng C, Schlegel HB. Isr J Chem 1993;33:449.
[36] Ochterski JW. Thermochemistry in Gaussian. http://www.gaussian.com Gaussian, Inc; 2000.
[37] Brookhart M, Green MLH. J Organomet Chem 1983;250:395.
[38] Ittel SD, Johnson LK, Brookhart M. Chem Rev 2000;100:1169–203.